Fibers and Polymers 2006, Vol.7, No.3, 276-285

Numerical Implementation of Modified Coulomb-Mohr Yield Criterion for Anisotropic and Asymmetric Materials

Myoung-Gyu Lee, Ji Hoon Kim, Hansun Ryou, Kwansoo Chung*, Jae Ryoun Youn, and Tae Jin Kang

School of Materials Science and Engineering, Seoul National University, Seoul 151-744, Korea
(Received June 29, 2006; Revised September 1, 2006; Accepted September 18, 2006)

Abstract: Development and numerical implementation for an elastoplastic constitutive model for anisotropic and asymmetric materials are presented in this paper. The Coulomb-Mohr yield criterion was modified to consider both the anisotropic and asymmetric properties. The modified yield criterion is an isotropic function of the principal values of a symmetric matrix which is linearly transformed from the Cauchy stress space. In addition to the constitutive equation, the numerical treatment for the singularity in the vertex region of yield surface and stress integration algorithm based on elastoplasticity were presented. In order to assess the accuracy of numerical algorithm, isoerror maps were considered. Also, extension of a strip with a circular hole was simulated and results compared with those obtained using the (smooth) Mises yield criterion to validate stress output for a complex stress state.

Keywords: Anisotropy, Asymmetry, Elastoplasticity, Coulomb-Mohr yield criterion

Introduction

Many engineering materials show different material behavior in the various directions. In addition to this anisotropic material property, some materials like fiber reinforced composites show different behavior between tension and compression properties. This difference in tension and compression is generally called asymmetry. In order to describe mechanical behavior of fiber reinforced composites using elastoplastic constitutive equations, both anisotropy and asymmetry should be considered.

In the traditional soil and rock mechanics, non-smooth yield surfaces have been used for describing the material properties using elastoplastic constitutive equations. In metal plasticity, the classical Tresca yield criterion is one of the simplest non-smooth yield surfaces. Unlike the smooth yield criterion like the Mises yield criterion, the non-smooth yield surface has corner points on the boundary of the elastic domain. Therefore, the normality rule of associate flow rule cannot uniquely determine the direction of plastic strain-rate. To ease this difficulty in numerical approach, Koiter suggested the definition of flow direction in the corner region [1]. Recently, a new computational model for the rate-independent elastoplastic materials with the Tresca yield surface and general nonlinear isotropic hardening was formulated and a numerical scheme for integration of the constitutive equations was suggested [2].

For the anisotropic yield function, Hill modified and extended the isotropic Mises yield function to the orthotropic functions [3]. Recently Barlat *et al.* proposed anisotropic yield functions especially for the aluminum alloys [4]. They used a linear transformation of the Cauchy stress in order to consider isotropic function. In order to consider both the anisotropy and asymmetry, the anisotropic yield function should be modified. One way to achieve asymmetry is to introduce the pressure dependent terms in the anisotropic yield function. By doing this, the yield surface will show different initial yield stress in tension and compression.

In this paper, the constitutive equation to describe the material behavior of composite materials was presented. To include the anisotropic as well as asymmetric properties of composites materials, the Coulomb-Mohr yield criterion was modified by introducing linear transformation matrix in which the anisotropic and asymmetric properties were included. This paper focused on the numerical algorithms, especially on the stress integration procedures for the finite element method. The numerical algorithm for the most challenging problem, numerical singularity in the region of vertex of yield surface, was developed on the basis of equivalent plastic work principle. In addition to stress update procedures, the algorithmic tangent modulus was obtained by differentiating the elastic stress-strain relationships and the discrete algorithmic flow rule. Though the developed constitutive equation fundamentally does not restrict the choice of hardening laws, the general nonlinear isotropic hardening and linear kinematic hardening were considered for simplicity. With minor modification, however, the presented theory and algorithms can be applied to the general combined nonlinear isotropic-kinematic hardening rules. The developed constitutive equations were implemented to the commercial finite element code ABAQUS/Standard. The accuracy of the numerical algorithm was assessed using the isoerror maps. Extension of strip with a circular hole was performed and compared with the results using the Mises yield surface to validate stress output for complex stress state.

*Corresponding author: kchung@snu.ac.kr

Modified Coulomb-Mohr Model

In the elastoplasticity theory, the strain increment is additively decomposed into elastic and plastic parts

$$d\boldsymbol{\varepsilon} = d\boldsymbol{\varepsilon}^e + d\boldsymbol{\varepsilon}^p \tag{1}$$

For orthotropic materials under plane-stress condition, the relation between Cauchy stress and elastic strain follows generalized Hook's law with their increments

$$\begin{pmatrix} d\sigma_x \\ d\sigma_y \\ d\sigma_{xy} \end{pmatrix} = \begin{bmatrix} \frac{E_x}{1-\nu_{xy}\nu_{yx}} & \frac{\nu_{yx}E_x}{1-\nu_{xy}\nu_{yx}} & 0 \\ \frac{\nu_{yx}E_x}{1-\nu_{xy}\nu_{yx}} & \frac{E_y}{1-\nu_{xy}\nu_{yx}} & 0 \\ 0 & 0 & G_{xy} \end{bmatrix} \begin{pmatrix} d\varepsilon_x^e \\ d\varepsilon_y^e \\ 2d\varepsilon_{xy}^e \end{pmatrix} \tag{2}$$

where E_x, E_y, ν_{xy}, ν_{yx} and G_{xy} are Young's moduli and Poisson's ratios and the shear modulus, respectively. To account for the asymmetry of the elastic behavior of the fiber reinforced composites, different values of Young's moduli are used for tensile and compressive modes, i.e.,

$$E_i = \begin{cases} E_i^T & \text{for} \quad \sigma_i \geq 0 \\ E_i^C & \text{for} \quad \sigma_i < 0 \end{cases} \quad \text{in } i\text{-direction, } i = x, y \tag{3}$$

where E_i^T and E_i^C are Young's moduli determined from tensile and compressive tests, respectively.

In order to describe anisotropic and asymmetric properties of yield surface, the Coulomb-Mohr yield surface was modified by incorporating anisotropic characteristics under plane stress condition. The original Coulomb-Mohr yield criterion under plane stress condition is given as (see Figure 1).

$$\begin{aligned} \Phi_1 &= s_1 - \bar{\sigma}_{iso} \\ \Phi_2 &= s_2 - \bar{\sigma}_{iso} \\ \Phi_3 &= -\frac{\bar{\sigma}_Y^t}{\bar{\sigma}_Y^c} s_1 + s_2 - \bar{\sigma}_{iso} \\ \Phi_4 &= -\frac{\bar{\sigma}_Y^t}{\bar{\sigma}_Y^c} s_1 - \bar{\sigma}_{iso} \\ \Phi_5 &= -\frac{\bar{\sigma}_Y^t}{\bar{\sigma}_Y^c} s_2 - \bar{\sigma}_{iso} \\ \Phi_6 &= s_1 - \frac{\bar{\sigma}_Y^t}{\bar{\sigma}_Y^c} s_2 - \bar{\sigma}_{iso} \end{aligned} \tag{4}$$

where $\bar{\sigma}_{iso}$ is the effective stress measuring the size of the yield surface and $\bar{\sigma}_Y^t$ and $\bar{\sigma}_Y^c$ are the initial yield strength in tension and compression, respectively. Anisotropy can be introduced with s_1, s_2 as the principal values tensor **s** which

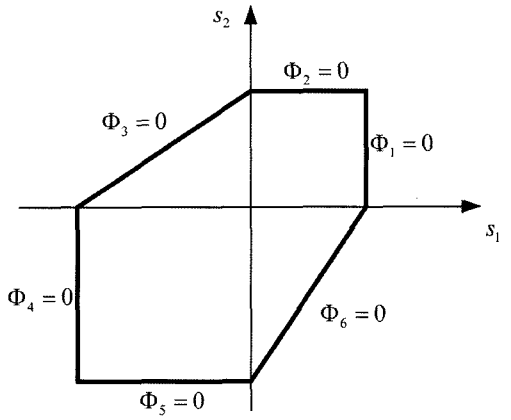

Figure 1. Yield criterion for anisotropic and asymmetric materials.

is obtained by the following linear transformation of Cauchy stress;

$$\mathbf{s} = \mathbf{T}\boldsymbol{\sigma} \tag{5}$$

where $\boldsymbol{\sigma}$ is Cauchy stress tensor and **T** is the linear transformation matrix which considers the anisotropy.

$$\mathbf{s} = \begin{bmatrix} s_{xx} \\ s_{yy} \\ s_{xy} \end{bmatrix} = \begin{bmatrix} 1 & 0 & 0 \\ 0 & \frac{\bar{\sigma}_{xY}^t}{\bar{\sigma}_{yY}^c} & 0 \\ 0 & 0 & c_{33} \end{bmatrix} \begin{bmatrix} \sigma_{xx} \\ \sigma_{yy} \\ \sigma_{xy} \end{bmatrix} = \mathbf{T}\boldsymbol{\sigma} \tag{6}$$

where $\bar{\sigma}_{xY}^t$ and $\bar{\sigma}_{yY}^c$ are initial yield stress in tension in the longitudinal (or equivalently fiber direction) and transverse direction, respectively. Here c_{33} represent the anisotropy coefficient for the shear component. This coefficient can be determined from the experiments containing shear stress component such as uniaxial tension tests loaded at 45 degree to the longitudinal direction. With the condition $\bar{\sigma}_{xY}^t = \bar{\sigma}_{yY}^c$, the yield criterion becomes equivalent to the Coulomb-Mohr criterion. The classical Tresca criterion is restored with further assumption, $\bar{\sigma}_Y^t = \bar{\sigma}_Y^c$. The transformed yield function considered in this paper is represented in Figure 1. Here, the yield function consists of 6 linear parts and each criterion is represented as $\Phi_{1\sim6}$. By using the developed yield criterion, the anisotropic and asymmetric properties can be effectively represented with the following limitation: The anisotropy of compression parts are determined from those of tensile parts. Therefore, the material properties needed to setup the criterion are two tensile yield strengths in each direction, one compressive yield strength and 45 degree uniaxial tensile yield stress. Figure 2 shows the tricomponent yield surface for an arbitrary material predicted with the current yield function. In this figure the stress for each directions is normalized with initial effective stress and the contours of normalized shear stress are drawn every 0.1. This figure shows the developed yield

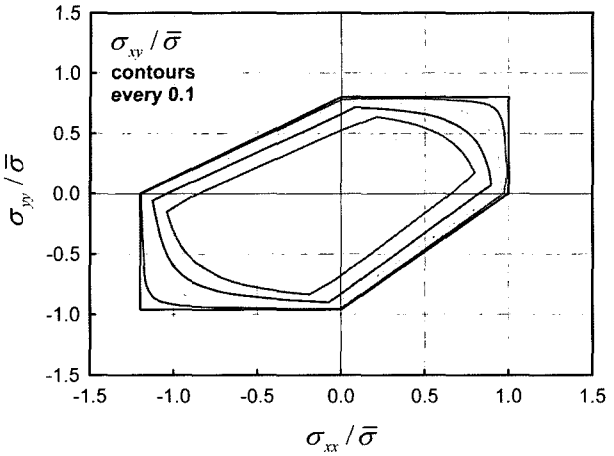

Figure 2. Tricomponent yield surface for modified Coulomb-Mohr criterion.

surface can describe the anisotropy as well as asymmetry.

As for the flow rule and loading/unloading conditions the associative normality rule has been generally applied in the plasticity field. Because, however, the current yield criterion is composed of non-smooth multi-surface, the corner region or vertex region cannot be differentiated so that a unique direction of plastic strain-rate does not exist. Here, the following flow rule, often referred to as Koiter's rule [1] is employed to consider the non-uniqueness of plastic strain-rate.

$$d\boldsymbol{\varepsilon}^p = \sum_{i=1}^{n} \gamma_i \frac{\partial \bar{\sigma}_i}{\partial \boldsymbol{\sigma}} \tag{7}$$

where $\bar{\sigma}_i$ and γ are active effective stress and plastic consistency parameter for each multi-surface, respectively and n is number of active yield surfaces. Therefore, for the plastic flow, two possible regions can be occurred in the trial stress space: edge region and vertex region which contains singular point by intersection of several surfaces. In the edge region, the active surface is uniquely determined and the yield function is differentiable, while more than two active surfaces exist in the vertex region so that special treatment should be made to determine yield surface normal. In Figure 3, the trial stress space outside the yield surface is divided by 19 different regions: six 1-surface regions, six 2-surface regions, six 3-surface regions and one 4-surface region for the current yield criterion.

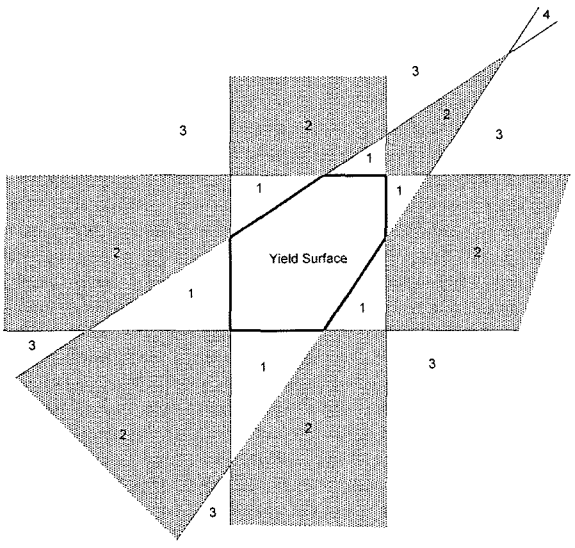

Figure 3. Number of active yield surfaces in trial stress space.

From the principle of plastic equivalent work along with nature of a first order homogeneous function, the increment of equivalent plastic strain-rate becomes

$$d\bar{\varepsilon} = \frac{\boldsymbol{\sigma} \cdot d\boldsymbol{\varepsilon}^p}{\bar{\sigma}(\boldsymbol{\sigma})} = \frac{\boldsymbol{\sigma} \cdot \sum_{i=1}^{n} \gamma_i \frac{\partial \bar{\sigma}_i}{\partial \boldsymbol{\sigma}}}{\bar{\sigma}(\boldsymbol{\sigma})} = \frac{\sum_{i=1}^{n} \gamma_i \bar{\sigma}_i}{\bar{\sigma}(\boldsymbol{\sigma})} \tag{8}$$

Therefore, the above equation results in $d\bar{\varepsilon} = \gamma$ for edge region ($n=1$) and $d\bar{\varepsilon} = \gamma_1 + \gamma_2$ for vertex region ($n=2$) and so on. equation (8) is useful when the effective stress does not have its conjugate strain explicitly defined with respect to the plastic strain increment [5].

In this paper, the combination of the isotropic hardening and linear kinematic hardening model is considered. Based on this hardening rule, the initial yield surface translates and expands simultaneously with plastic deformation. The yield surface in Cauchy stress space is described,

$$\tilde{\Phi}_i(\boldsymbol{\sigma} - \boldsymbol{\alpha}, \bar{\sigma}_{iso}) = 0 \quad (i = 1 \sim 6) \tag{9}$$

where $\boldsymbol{\alpha}$ is the back-stress by which the current yield stress surface is translated from an initial position. Here, $\bar{\sigma}_{iso}$ is the effective stress and a function of equivalent plastic strain.

As for the translation of the yield stress surface by the kinematic hardening, the linear kinematic hardening suggested by Prager [6] or Ziegler [7] was assumed. In the formal model the yield surface moves in the direction of loading, while in the direction of plastic strain-rate for the latter model. The well-known evolution rules for the two models are

$$d\boldsymbol{\alpha} = K d\boldsymbol{\varepsilon}^p \qquad \text{for Prager model} \tag{10}$$

$$d\boldsymbol{\alpha} = K d\bar{\varepsilon} \frac{\boldsymbol{\sigma} - \boldsymbol{\alpha}}{\bar{\sigma}_{iso}} \qquad \text{for Ziegler model} \tag{11}$$

where K is the kinematic hardening modulus and $d\boldsymbol{\varepsilon}^p$ is the plastic strain increment and $d\bar{\varepsilon}$ is the effective plastic strain increment.

Numerical Implementation of Modified Coulomb-Mohr Model

The numerical scheme to solve nonlinear boundary value problems using the finite element method is to iteratively try

out discrete displacement increment at the discretized material space and process time until the trial values ultimately satisfy either the static or dynamic principle of momentum at every material element. At the first step, the discrete strain increments are calculated from trial displacement increments and then at the second step, the stresses and other state variables such as plastic strains, back stresses are updated from the discrete strain increments using the elastoplastic constitutive equation. Finally, the tolerance is checked whether the static or dynamic principle of momentum is satisfied.

For a given strain increment $\Delta\boldsymbol{\varepsilon}$, the numerical formulation provides $\Delta\boldsymbol{\varepsilon}^e$, $\Delta\boldsymbol{\varepsilon}^p$ and $\Delta\boldsymbol{\sigma}$, $\Delta\boldsymbol{\alpha}$, which are

$$\Delta\boldsymbol{\varepsilon}^p = \sum_{i=1}^{n} \gamma_i \frac{\partial \bar{\sigma}_i}{\partial(\boldsymbol{\sigma}-\boldsymbol{\alpha})} \tag{12}$$

$$\Delta\boldsymbol{\varepsilon}^e = \Delta\boldsymbol{\varepsilon} - \Delta\boldsymbol{\varepsilon}^p \tag{13}$$

$$\Delta\boldsymbol{\sigma} = \mathbf{C}\cdot\Delta\boldsymbol{\varepsilon}^e = \mathbf{C}\cdot(\Delta\boldsymbol{\varepsilon}-\Delta\boldsymbol{\varepsilon}^p) \tag{14}$$

$$\Delta\boldsymbol{\alpha} = K\Delta\bar{\varepsilon}\frac{(\boldsymbol{\sigma}-\boldsymbol{\alpha})}{\bar{\sigma}_{iso}} \quad \text{or} \quad \Delta\boldsymbol{\alpha} = K\Delta\boldsymbol{\varepsilon}^p \tag{15}$$

where $\mathbf{C}$ and K are the anisotropic elasticity matrix and the kinematic hardening modulus, respectively.

Note here that all these increments are function of unknown quantity $\Delta\bar{\varepsilon}$ when the hardening curve is provided. The unknown $\Delta\bar{\varepsilon}$ can be obtained from the following consistency requirement.

$$\bar{\sigma}_i(\boldsymbol{\sigma}_0 - \boldsymbol{\alpha}_0 + \Delta\boldsymbol{\sigma} - \Delta\boldsymbol{\alpha}) = \bar{\sigma}_{iso}(\bar{\varepsilon}_0 + \Delta\bar{\varepsilon}) \quad (i = 1\sim6) \tag{16}$$

where the subscript "0" represents the (initial) values of the previous step and the right-hand side value is obtained from the measured hardening curve.

Based on the constitutive equations developed here, the stress update scheme is outlined using the predictor-corrector method based on the Newton-Raphson method. The updated stress is initially assumed to be elastic for a given discrete strain increment $\Delta\boldsymbol{\varepsilon}$. Therefore,

$$\boldsymbol{\sigma}_{n+1}^T = \boldsymbol{\sigma}_n + \mathbf{C}\Delta\boldsymbol{\varepsilon} \tag{17}$$

where the superscript "T" stands for a trial state and the subscript denotes the process time step. Also, preserving the plastic quantities as the previous values,

$$\bar{\varepsilon}_{n+1}^T = \bar{\varepsilon}_n \quad \text{and} \quad \boldsymbol{\alpha}_{n+1}^T = \boldsymbol{\alpha}_n \tag{18}$$

If the following yield condition is satisfied with the trial values for a prescribed elastic tolerance Tol^e for each active surface,

$$\Phi_i = \bar{\sigma}_i(\boldsymbol{\sigma}_{n+1}^T - \boldsymbol{\alpha}_{n+1}^T) - \bar{\sigma}_{iso}(\bar{\varepsilon}_{n+1}^T) < \text{Tol}^e \tag{19}$$

the process at the step n+1 is considered elastic.

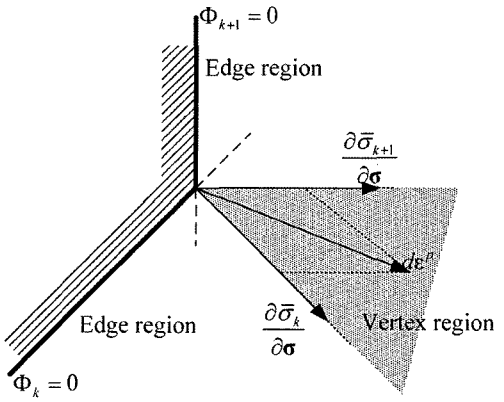

Figure 4. Plastic strain increment in the edge and vertex regions.

If the above condition on yielding is violated ($\Phi_i > \text{Tol}^e$), the step is considered elastoplastic and the trial elastic stress state is taken as an initial value for the solution of the plastic corrector problem until the yield condition is satisfied during the iteration. The predictor-corrector scheme based on the Newton-Raphson method was used to solve $\Delta\bar{\varepsilon}$. The elastic trial stress falls within one of 19 regions as described in Figure 3. In the current numerical algorithm, if stress falls in 3- or 4-surface regions, one or two surfaces which has the smallest value of residual (Φ_i) during iterations are excluded for the numerical convenience. Therefore, only 1-surface or 2-surface regions are considered in the current stress update algorithm. In summary, the stress during the iteration can experience one of the following regions starting from trial stress.

$$\begin{array}{l} 4\rightarrow2 \quad \text{or} \quad 4\rightarrow2\rightarrow1 \\ 3\rightarrow2 \quad \text{or} \quad 3\rightarrow2\rightarrow1 \\ 2\rightarrow1 \end{array} \tag{20}$$

where figures mean the number of active surfaces.

If the stress falls into the vertex regions, the two consistency conditions should be satisfied at the same time in these regions as shown in Figure 4. Note that single unique normal direction exists in the edge region so that the same procedure can be applied with one consistency condition. Let Φ_k and Φ_{k+1} are two active yield surfaces and the updated stress lies at the vertex. Then the two nonlinear consistency equations are

$$\Phi_i = \bar{\sigma}_i(\boldsymbol{\sigma}-\boldsymbol{\alpha}) - \bar{\sigma}_{iso}(\gamma_k + \gamma_{k+1}) = 0 \quad (i = k \text{ or } k+1) \tag{21}$$

where

$$\boldsymbol{\sigma}_{n+1} = \boldsymbol{\sigma}_{n+1}^T - \mathbf{C}\cdot\sum_{i=k}^{k+1}\gamma_i\frac{\partial\bar{\sigma}_k}{\partial(\boldsymbol{\sigma}_{n+\beta}-\boldsymbol{\alpha}_{n+\beta})} \tag{22}$$

and

$$\boldsymbol{\alpha}_{n+1} = \boldsymbol{\alpha}_n + K\frac{(\boldsymbol{\sigma}-\boldsymbol{\alpha})}{\bar{\sigma}_{iso}}(\gamma_k + \gamma_{k+1}) \quad \text{or}$$

$$\boldsymbol{\alpha}_{n+1} = \boldsymbol{\alpha}_n + K\sum_{i=k}^{i=k+1}\gamma_i \frac{\partial \bar{\sigma}_i}{\partial(\boldsymbol{\sigma}_{n+\beta}-\boldsymbol{\alpha}_{n+\beta})} \tag{23}$$

where $0 \le \beta \le 1$. From the linearized form of equation (21),

$$\delta\begin{pmatrix}\gamma_k\\ \gamma_{k+1}\end{pmatrix}^{(m+1)} = -\begin{bmatrix}\frac{\partial\Phi_k}{\partial\gamma_k} & \frac{\partial\Phi_k}{\partial\gamma_{k+1}}\\ \frac{\partial\Phi_{k+1}}{\partial\gamma_k} & \frac{\partial\Phi_{k+1}}{\partial\gamma_{k+1}}\end{bmatrix}_{(m)}^{-1}\begin{pmatrix}\Phi_k\\ \Phi_{k+1}\end{pmatrix}_{(m)}$$

$$= \frac{1}{\frac{\partial\Phi_k}{\partial\gamma_{k+1}}\frac{\partial\Phi_{k+1}}{\partial\gamma_k}-\frac{\partial\Phi_k}{\partial\gamma_k}\frac{\partial\Phi_{k+1}}{\partial\gamma_k}}\begin{bmatrix}\frac{\partial\Phi_{k+1}}{\partial\gamma_{k+1}} & -\frac{\partial\Phi_k}{\partial\gamma_{k+1}}\\ -\frac{\partial\Phi_{k+1}}{\partial\gamma_k} & \frac{\partial\Phi_k}{\partial\gamma_k}\end{bmatrix}_{(m)}\begin{pmatrix}\Phi_k\\ \Phi_{k+1}\end{pmatrix}_{(m)} \tag{24}$$

for the m-th iteration and

$$\frac{\partial\Phi_i}{\partial\gamma_i} = \frac{\partial\Phi_i}{\partial\boldsymbol{\sigma}}\frac{\partial\boldsymbol{\sigma}}{\partial\gamma_i} + \frac{\partial\Phi_i}{\partial\boldsymbol{\alpha}}\frac{\partial\boldsymbol{\alpha}}{\partial\gamma_i} + \frac{\partial\Phi_i}{\partial\bar{\sigma}_{iso}}\frac{\partial\bar{\sigma}_{iso}}{\partial\gamma_i} \quad (i=k \text{ or } k+1) \tag{25}$$

where

$$\frac{\partial\boldsymbol{\sigma}_{n+1}}{\partial\gamma_i} = -\mathbf{C}\cdot\frac{\partial\bar{\sigma}_i}{\partial(\boldsymbol{\sigma}_{n+\beta}-\boldsymbol{\alpha}_{n+\beta})} \quad (i=k \text{ or } k+1) \tag{26}$$

$$\frac{\partial\boldsymbol{\alpha}_{n+1}}{\partial\gamma_i} = K\cdot\frac{(\boldsymbol{\sigma}_{n+\beta}-\boldsymbol{\alpha}_{n+\beta})}{\bar{\sigma}_{iso}} \quad \text{or}$$

$$\frac{\partial\boldsymbol{\alpha}_{n+1}}{\partial\gamma_i} = K\cdot\frac{\partial\bar{\sigma}_i}{\partial(\boldsymbol{\sigma}_{n+\beta}-\boldsymbol{\alpha}_{n+\beta})} \quad (i=k \text{ or } k+1) \tag{27}$$

while

$$\frac{\partial\Phi_i}{\partial\boldsymbol{\sigma}_{n+1}} = -\frac{\partial\Phi_i}{\partial\boldsymbol{\alpha}_{n+1}} = \frac{\partial\bar{\sigma}_i}{\partial(\boldsymbol{\sigma}_{n+1}-\boldsymbol{\alpha}_{n+1})}, \text{ and } \frac{\partial\Phi_i}{\partial\bar{\sigma}_{iso}} = -1 \tag{28}$$

Note that in deriving equation (27), the higher order terms caused by the variation of stresses with respect to the variation of the effective strain increment have been ignored for simplicity.

Since the current yield criterion is expressed in terms of principal stress space of **s** for the plane stress condition, the equivalent stress $\bar{\sigma}(\boldsymbol{\sigma})$ and its first derivative $\partial\bar{\sigma}/\partial\boldsymbol{\sigma}$ should be calculated from given Cauchy stress state, $(\sigma_{xx}, \sigma_{yy}, \sigma_{xy})^T$. For the plane stress condition, the principal values are calculated with equation (5),

$$s_{1,2} = \frac{s_{xx}+s_{yy}}{2} \pm \sqrt{\left(\frac{s_{xx}-s_{yy}}{2}\right)^2 + s_{xy}^2} \tag{29}$$

If we assume the associate flow rule, the normal to the yield surface, which is needed to calculate the plastic strain-rate, is obtained with some manipulations;

$$\mathbf{m} = \begin{bmatrix}\frac{\partial\bar{\sigma}_i}{\partial\sigma_{xx}}\\ \frac{\partial\bar{\sigma}_i}{\partial\sigma_{yy}}\\ \frac{\partial\bar{\sigma}_i}{\partial\sigma_{xy}}\end{bmatrix} = \begin{bmatrix}\frac{\partial\bar{\sigma}_i}{\partial s_1}\frac{\partial s_1}{\partial s_{xx}}\frac{\partial s_{xx}}{\partial\sigma_{xx}} + \frac{\partial\bar{\sigma}_i}{\partial s_2}\frac{\partial s_2}{\partial s_{xx}}\frac{\partial s_{xx}}{\partial\sigma_{xx}}\\ \frac{\partial\bar{\sigma}_i}{\partial s_1}\frac{\partial s_1}{\partial s_{yy}}\frac{\partial s_{yy}}{\partial\sigma_{yy}} + \frac{\partial\bar{\sigma}_i}{\partial s_2}\frac{\partial s_2}{\partial s_{yy}}\frac{\partial s_{yy}}{\partial\sigma_{yy}}\\ \frac{\partial\bar{\sigma}_i}{\partial s_1}\frac{\partial s_1}{\partial s_{xy}}\frac{\partial s_{xy}}{\partial\sigma_{xy}} + \frac{\partial\bar{\sigma}_i}{\partial s_2}\frac{\partial s_2}{\partial s_{xy}}\frac{\partial s_{xy}}{\partial\sigma_{xy}}\end{bmatrix} \tag{30}$$

where

$$\left[\frac{\partial s_p}{\partial s_{\alpha\beta}}\right]_{p=1\sim2 \text{ and } \alpha,\beta=x,y} = \begin{bmatrix}\frac{\partial s_1}{\partial s_{xx}} & \frac{\partial s_2}{\partial s_{xx}}\\ \frac{\partial s_1}{\partial s_{yy}} & \frac{\partial s_2}{\partial s_{yy}}\\ \frac{\partial s_1}{\partial s_{xy}} & \frac{\partial s_2}{\partial s_{xy}}\end{bmatrix}$$

$$= \begin{bmatrix}\frac{1}{2}+\frac{s_{xx}-s_{yy}}{4\Delta} & \frac{1}{2}-\frac{s_{xx}-s_{yy}}{4\Delta}\\ \frac{1}{2}-\frac{s_{xx}-s_{yy}}{4\Delta} & \frac{1}{2}+\frac{s_{xx}-s_{yy}}{4\Delta}\\ \frac{s_{xy}}{\Delta} & -\frac{s_{xy}}{\Delta}\end{bmatrix}_{3\times2} \tag{31}$$

with

$$\Delta = \sqrt{\left(\frac{s_{xx}-s_{yy}}{2}\right)^2 + s_{xy}^2} \tag{32}$$

and

$$\left[\frac{\partial\bar{\sigma}_i}{\partial s_p}\right]_{p=1\sim2} = [n_1, n_2]^i \tag{33}$$

where

$$[n_1,n_2]^i = (1,0),\ (0,1),\ \left(-\frac{\bar{\sigma}_Y^t}{\bar{\sigma}_Y^c}, 1\right),\ \left(-\frac{\bar{\sigma}_Y^t}{\bar{\sigma}_Y^c}, 0\right)$$

$$\left(0, -\frac{\bar{\sigma}_Y^t}{\bar{\sigma}_Y^c}\right),\ \left(1, -\frac{\bar{\sigma}_Y^t}{\bar{\sigma}_Y^c}\right) \quad \text{for} \quad i=1\sim6 \tag{34}$$

and from the equation (6),

$$\left[\frac{\partial s_{\alpha\beta}}{\partial\sigma_{\gamma\delta}}\right] = \begin{bmatrix}\frac{\partial s_{xx}}{\partial\sigma_{xx}} & 0 & 0\\ 0 & \frac{\partial s_{yy}}{\partial\sigma_{yy}} & 0\\ 0 & 0 & \frac{\partial s_{xy}}{\partial\sigma_{xy}}\end{bmatrix} = \begin{bmatrix}1 & 0 & 0\\ 0 & \frac{\bar{\sigma}_{xY}^T}{\bar{\sigma}_{yY}^T} & 0\\ 0 & 0 & c_{33}\end{bmatrix} \tag{35}$$

After obtaining consistency parameters from the above procedures, the stress and other plastic state variables can be

updated.

$$\Delta\bar{\varepsilon}_{n+1}^{(m+1)} = \Delta\bar{\varepsilon}_{n+1}^{(m)} + \delta(\Delta\bar{\varepsilon}) = \begin{cases} \Delta\bar{\varepsilon}_{n+1}^{(m)} + \delta(\gamma) & \text{(1-surface region)} \\ \Delta\bar{\varepsilon}_{n+1}^{(m)} + \delta(\gamma_1+\gamma_2) & \text{(2-surface region)} \end{cases} \tag{36}$$

$$\boldsymbol{\sigma}_{n+1}^{(m+1)} = \boldsymbol{\sigma}_{n+1}^{(m)} + \Delta\boldsymbol{\sigma}_{n+1}(\Delta\boldsymbol{\varepsilon}_{n+1}^{(m+1)}) \tag{37}$$

$$\boldsymbol{\alpha}_{n+1}^{(m+1)} = \boldsymbol{\alpha}_{n+1}^{(m)} + \Delta\boldsymbol{\alpha}_{n+1}(\Delta\boldsymbol{\varepsilon}_{n+1}^{(m+1)}) \tag{38}$$

Tangent modulus consistent with the integration algorithm developed above is needed to preserve the quadratic rate of convergence that characterizes Newton's method [8]. With the current yield criterion, the two different consistent tangent modulus should be considered with an associate stress update algorithm to the two different regions explained before. Since the algorithm for the edge region is subset of that of vertex region (2-surface region), only the procedure for the vertex region is presented. In order to calculate algorithmic tangent modulus, the differentiations of stress and back stress are performed.

$$d\boldsymbol{\sigma}_{n+1} = \mathbf{C}\cdot\left[d\boldsymbol{\varepsilon}_{n+1} - \sum_{i=k}^{k+1} d\gamma_i \frac{\partial\bar{\sigma}_i}{\partial(\boldsymbol{\sigma}_{n+1}-\boldsymbol{\alpha}_{n+1})}\right] \tag{39}$$

$$d\boldsymbol{\alpha}_{n+1} = K\sum_{i=k}^{k+1} d\gamma_i \frac{\partial\bar{\sigma}_i}{\partial(\boldsymbol{\sigma}_{n+1}-\boldsymbol{\alpha}_{n+1})} \tag{40}$$

or

$$d\boldsymbol{\alpha}_{n+1} = Kd\bar{\varepsilon}\frac{(\boldsymbol{\sigma}_{n+1}-\boldsymbol{\alpha}_{n+1})}{\bar{\sigma}_{iso}}d\boldsymbol{\sigma}_{n+1} + K\frac{(\boldsymbol{\sigma}_{n+1}-\boldsymbol{\alpha}_{n+1})}{\bar{\sigma}_{iso}+Kd\bar{\varepsilon}}(d\gamma_1+d\gamma_2)\left[1-\frac{\bar{H}d\bar{\varepsilon}}{\bar{\sigma}_{iso}}\right] \tag{41}$$

Note that the derivatives of yield surface normal $\partial^2\bar{\sigma}/\partial\boldsymbol{\sigma}\partial\boldsymbol{\sigma}$ shown in the common implicit formulation are not included in equation (40) because these values are vanishing for the current yield criterion.

Differentiating the two active consistency conditions at time step $n+1$ and substituting equations. (39) and (40) yield the following linearized simultaneous equations.

$$d\Phi_i = \frac{\partial\bar{\sigma}_i}{\partial(\boldsymbol{\sigma}_{n+1}-\boldsymbol{\alpha}_{n+1})}(d\boldsymbol{\sigma}_{n+1}-d\boldsymbol{\alpha}_{n+1}) - d\bar{\sigma}_{iso} = \mathbf{m}_{n+1}^{i}\mathbf{C}d\boldsymbol{\varepsilon}_{n+1} - D_{i1}d\gamma_k - D_{i2}d\gamma_{k+1} = 0 \quad (i=k \text{ or } k+1) \tag{42}$$

where $\mathbf{m}_{n+1}^{i} = \dfrac{\partial\bar{\sigma}_i}{\partial(\boldsymbol{\sigma}_{n+1}-\boldsymbol{\alpha}_{n+1})}$ and the parameters are

$$D_{i1} = \mathbf{m}_{n+1}^{i}\cdot\mathbf{C}\cdot\mathbf{m}_{n+1}^{k} + K\mathbf{m}_{n+1}^{i}\cdot\mathbf{m}_{n+1}^{k} + \bar{H} \tag{43}$$

$$D_{i2} = \mathbf{m}_{n+1}^{i}\cdot\mathbf{C}\cdot\mathbf{m}_{n+1}^{k+1} + K\mathbf{m}_{n+1}^{i}\cdot\mathbf{m}_{n+1}^{k+1} + \bar{H} \tag{44}$$

for Prager back stress evolution rule and

$$D_{i1} = \mathbf{m}_{n+1}^{i}\cdot\mathbf{C}\cdot\mathbf{m}_{n+1}^{k} - \frac{K\bar{H}}{\bar{\sigma}_{iso}}d\bar{\varepsilon} + K + \frac{\bar{H}}{A} \tag{45}$$

$$D_{i2} = \mathbf{m}_{n+1}^{i}\cdot\mathbf{C}\cdot\mathbf{m}_{n+1}^{k+1} - \frac{K\bar{H}}{\bar{\sigma}_{iso}}d\bar{\varepsilon} + K + \frac{\bar{H}}{A} \tag{46}$$

with

$$\bar{H} = \frac{d\bar{\sigma}_{iso}}{d\bar{\varepsilon}}, \quad A = \frac{\bar{\sigma}_{iso}}{\bar{\sigma}_{iso}+Kd\bar{\varepsilon}} \tag{47}$$

for Ziegler back stress evolution rule, respectively.

By solving two equations, the consistency parameters for the vertex region are obtained as follows,

$$\begin{bmatrix} d\lambda_1 \\ d\lambda_2 \end{bmatrix} = \frac{1}{D_{(k)1}D_{(k+1)2} - D_{(k)2}D_{(k+1)1}}\begin{bmatrix} D_{(k+1)2} & -D_{(k)2} \\ -D_{(k+1)1} & D_{(k)1} \end{bmatrix} \begin{pmatrix} \mathbf{m}_{n+1}^{k}\cdot\mathbf{C}\cdot d\boldsymbol{\varepsilon}_{n+1} \\ \mathbf{m}_{n+1}^{k+1}\cdot\mathbf{C}\cdot d\boldsymbol{\varepsilon}_{n+1} \end{pmatrix} \tag{48}$$

Substituting equation (48) into equation (39) gives the consistent tangent modulus, i.e.,

$$d\boldsymbol{\sigma}_{n+1} = \mathbf{C}^{ep}\cdot d\boldsymbol{\varepsilon}_{n+1} \tag{49}$$

where

$$\mathbf{C}^{ep} = \mathbf{C} - \frac{D_{(k+1)2}\mathbf{C}\mathbf{m}_{n+1}^{k}\otimes\mathbf{C}\mathbf{m}_{n+1}^{k} - D_{(k)2}\mathbf{C}\mathbf{m}_{n+1}^{k+1}\otimes\mathbf{C}\mathbf{m}_{n+1}^{k}}{\bar{\Delta}} - \frac{D_{(k)1}\mathbf{C}\mathbf{m}_{n+1}^{k+1}\otimes\mathbf{C}\mathbf{m}_{n+1}^{k+1} - D_{(k+1)1}\mathbf{C}\mathbf{m}_{n+1}^{k}\otimes\mathbf{C}\mathbf{m}_{n+1}^{k+1}}{\bar{\Delta}} \tag{50}$$

where

$$\bar{\Delta} = D_{(k)1}D_{(k+1)2} - D_{(k)2}D_{(k+1)1} \tag{51}$$

Here, $\otimes$ represents tensor product.

In this paper, based on the numerical formulations developed here, the constitutive law for the modified Tresca criterion was implemented into the commercial finite element code ABAQUS/Standard using the implicit user subroutine UMAT. Note that all stresses, strains, and state variables are defined in the local material axes for anisotropic materials. These local material axes form a basis system in which stress and strain components are stored. This represents a co-rotational coordinate system in which the basis system rotates with the material. At the beginning of stress update routine in UMAT, the given stress and strain are automatically rotated values in the co-rotated coordinate system but the other state variables such as back stress and plastic strain should be rotated to account for the evolution of the material directions. The rotation effect is treated using the rotation matrix which is decomposed from the deformation gradient

tensor ($\mathbf{R}=\mathbf{F}\mathbf{U}^{-1}$). The procedure is summarized below.

- Given variables: strain increment at the current time step, $\Delta\boldsymbol{\varepsilon}$ and stress and back stress, $\boldsymbol{\sigma}_n$, $\boldsymbol{\alpha}_n$, plastic strain and equivalent plastic strain $\boldsymbol{\varepsilon}_n^p$ and $\bar{\varepsilon}_n^p$
- To be determined: stress and back stress $\boldsymbol{\sigma}_{n+1}$, $\boldsymbol{\alpha}_{n+1}$ and increment of equivalent plastic strain $\Delta\bar{\varepsilon}_{n+1}^p$ for the next time step.
- Step 1: Calculate trial elastic stress

$$\boldsymbol{\sigma}_{n+1}^T = \boldsymbol{\sigma}_n + \mathbf{C}\Delta\boldsymbol{\varepsilon}$$

- Step 2: Check the yield condition
  If $\Phi_i < \mathrm{Tol}^e$ for all surfaces $i = 1\sim6$ then set $(\bullet)_{n+1} = (\bullet)^{\mathrm{trial}}{}_{n+1}$ and Exit.
  Else
  Check active yield surface and set number of active surface (n)
  If n=3 or 4, exclude surfaces which have smallest residual
  Set, $\boldsymbol{\sigma}_{n+1}^0 = \boldsymbol{\sigma}_{n+1}^T$, $\boldsymbol{\sigma}_{n+1}^0 = \boldsymbol{\alpha}_n$, $\Delta\bar{\varepsilon}_{n+1}^p = \bar{\varepsilon}_n^p$, $\Delta\gamma_i = 0$
  Go to next step
- Step 3: Evaluate the addition to the equivalent plastic strain increment by equation (22)

$$\delta\begin{pmatrix}\gamma_k\\ \gamma_{k+1}\end{pmatrix}^{(m+1)} = \frac{1}{\dfrac{\partial\Phi_k}{\partial\gamma_{k+1}}\dfrac{\partial\Phi_{k+1}}{\partial\gamma_k} - \dfrac{\partial\Phi_k}{\partial\gamma_k}\dfrac{\partial\Phi_{k+1}}{\partial\gamma_{k+1}}}\begin{bmatrix}\dfrac{\partial\Phi_{k+1}}{\partial\gamma_{k+1}} & -\dfrac{\partial\Phi_k}{\partial\gamma_{k+1}}\\ -\dfrac{\partial\Phi_{k+1}}{\partial\gamma_k} & \dfrac{\partial\Phi_k}{\partial\gamma_k}\end{bmatrix}_{(m)}\begin{pmatrix}\Phi_k\\ \Phi_{k+1}\end{pmatrix}_{(m)}$$

  for 2-surface region and $\lambda_{k+1} = 0$, $\Phi_{k+1} = 0$ for edge region.
  If $\delta\lambda_{k\text{ or }k+1} < 0$ then set n=1 and go to Step 3
- Step 4: Update variables and convergence check

$$\boldsymbol{\sigma}_{n+1}^{(m+1)} = \boldsymbol{\sigma}_{n+1}^{(m)} + \Delta\boldsymbol{\sigma}_{n+1}^{(m+1)}$$

$$\boldsymbol{\alpha}_{n+1}^{(m+1)} = \boldsymbol{\alpha}_{n+1}^{(m)} + \Delta\boldsymbol{\alpha}_{n+1}^{(m+1)}$$

$$\Delta\gamma_i^{(m+1)} = \Delta\gamma_i^{(m)} + \delta\gamma_i^{(m+1)}$$

  Check convergence: if $\Phi_i^{(m+1)} < \mathrm{Tol}^c$ then go to Step 5, else go to Step 3
- Step 5: Calculate consistent tangent modulus
  Calculate algorithmic tangent modulus and go to next time step

---

Numerical Verifications

The objective of this section is to assess the formulation and numerical algorithms considered in this paper. To this end, isoerror maps have been used based on a strain-controlled homogeneous problem and this technique can assess the overall accuracy of the algorithm [8]. Three points on the yield surface are chosen representing a wide range of possible states of stress. The three points are labeled A, B and C in Figure 5, which correspond to uniaxial, biaxial and pure shear stress state, respectively. In order to calculate the isoerror maps for each point on the yield surface the sequence of specified normalized strain increments are considered. The corresponding stresses to the prescribed strains are calculated applying the developed stress integration algorithm. Here, for simplicity but without loss of generality, the calculation was performed with respect to principal values of the strain and stress tensors, which are adopted elsewhere [9]. The isoerror maps are plotted as the root mean square of the error between exact and computed solution as following:

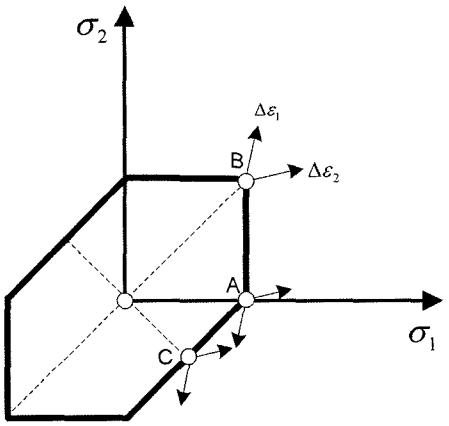

Figure 5. Plane stress yield surface and points for isoerror maps.

$$e \equiv \frac{\sqrt{(\boldsymbol{\sigma}-\boldsymbol{\sigma}^{exact}):(\boldsymbol{\sigma}-\boldsymbol{\sigma}^{exact})}}{\sqrt{\boldsymbol{\sigma}^{exact}\cdot\boldsymbol{\sigma}^{exact}}} \times 100(\%) \qquad (52)$$

where $\boldsymbol{\sigma}$ and $\boldsymbol{\sigma}^{exact}$ are the calculated stress by applying the developed algorithm and the exact solution which is obtained by repeatedly applying the algorithm with 1000 subincrements. The calculated isoerror maps for three points A, B and C are shown in Figure 6. The classical Tresca yield criterion by adjusting material parameters of modified Coulomb-Mohr model with no hardening and isotropic linear elastic constitutive equation with Young's modulus 70 GPa and Poisson's ratio of 0.3 was used for simplicity. This condition is the same as reported in the previous work (Simo and Hughes, 1998) with von Mises yield surface except for the shape of yield surface. For all three stress states, the exact solutions are widely distributed. In case of biaxial stress state, especially, the exact solutions for any strain increments were obtained with small numerical errors. This is because the stress update is performed in the vertex region and the updated stress is placed in the corner exactly.

As a second example, the extension of a strip with a circular hole is considered to illustrate the performance of the developed numerical algorithms for the non-smooth yield criterion. Due to the hole in a specimen considerable complex stress distribution will be generated and therefore this example can play an adequate role for assessing the validity of developed constitutive equations and numerical algorithms. Computations are performed with a general purpose, nonlinear finite element program ABAQUS with user material subroutine UMAT. The conditions are the same as the previous example except for the hardening equations and elastic behavior below.

$$\bar{\sigma}_{iso} = \bar{\sigma}_0 + a(1-\exp(-b\bar{\varepsilon})) \quad \text{and} \quad K = 0 \tag{53}$$

The geometry and finite element mesh for the problem is shown in Figure 7. The thickness of the shell element is unit

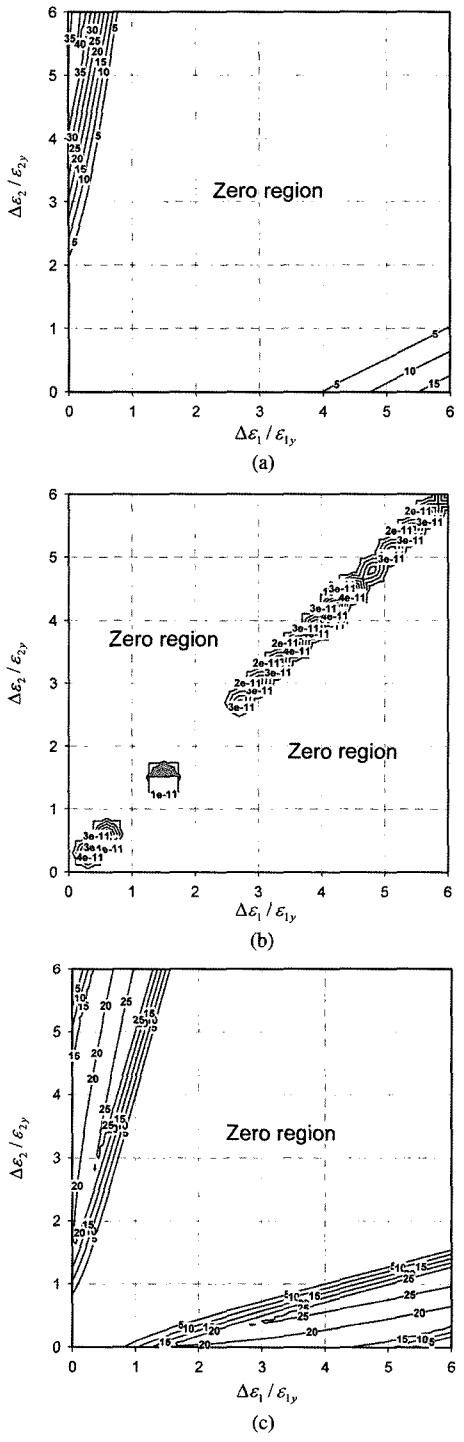

Figure 6. Isoerror maps under (a) uniaxial, (b) biaxial, and (c) pure shear stress states.

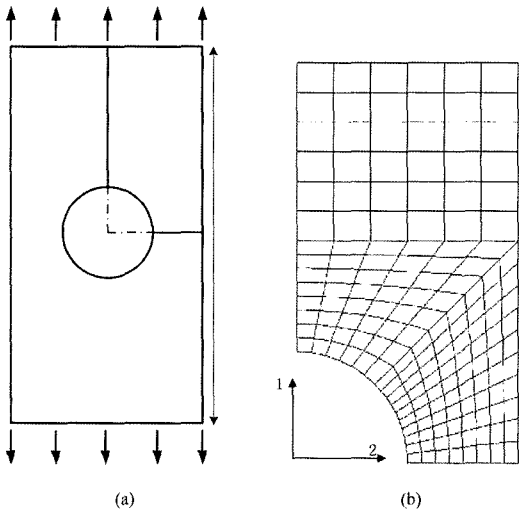

Figure 7. Plane stress strip with a circular hole with uniform displacement; (a) schematic view, (b) finite element model of a quarter of specimen.

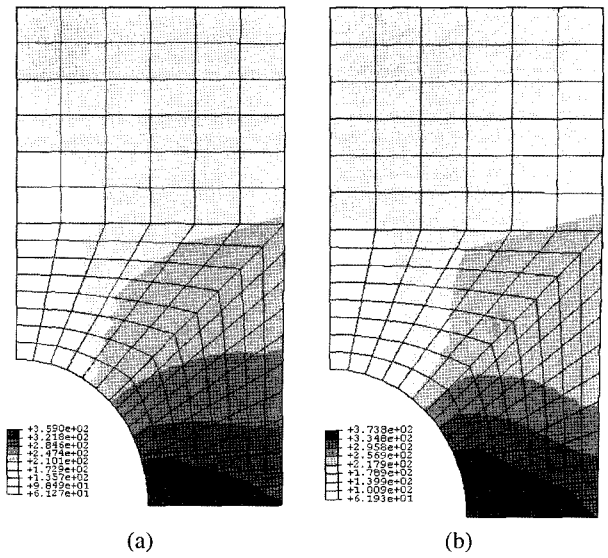

Figure 8. Stress component σ_{11}; (a) non-smooth yield surface (Tresca), (b) smooth yield surface (Mises).

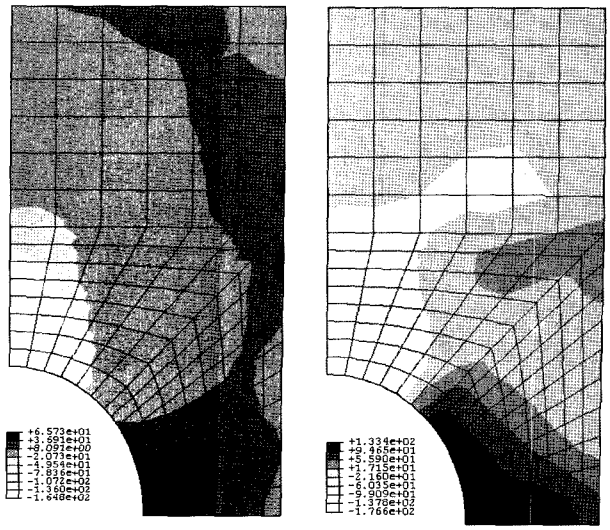

(a) (b)

Figure 9. Stress component σ_{22}; (a) non-smooth yield surface (Tresca), (b) smooth yield surface (Mises).

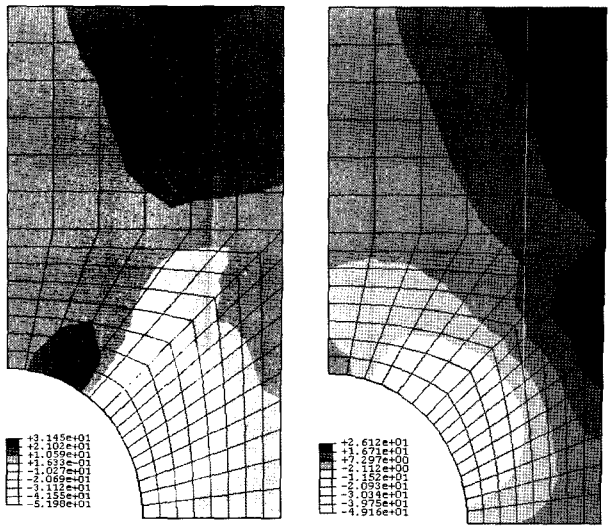

(a) (b)

Figure 10. Stress component σ_{12}; (a) non-smooth yield surface (Tresca), (b) smooth yield surface (Mises).

value and the uniform displacement is applied as a boundary conditions. Using the symmetry condition only one quarter of the specimen is analyzed. As for the element, 164 four node reduced shell elements (S4R) was used in the calculation. The calculation showed that the problem was generally solved with reasonable rate of convergence both in the global Newton solution procedure and in the material subroutine. For the comparison purpose, three stress component σ_{11}, σ_{22}, σ_{12} and effective plastic strain distributions are compared with those of von Mises yield surface as shown in Figures 8-11. As can be seen from these figures, the results

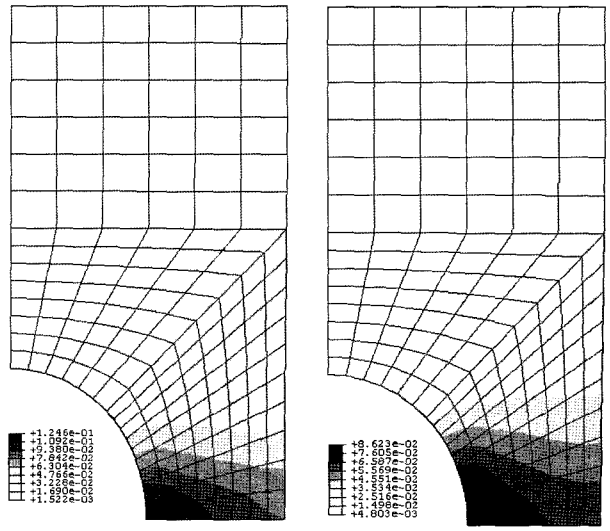

(a) (b)

Figure 11. Effective plastic strain $\bar{\varepsilon}^p$; (a) non-smooth yield surface (Tresca), (b) smooth yield surface (Mises).

show very similar distribution even though some deviation in the absolute values.

From the above two examples, we can conclude that the developed yield criterion and numerical algorithms for the non-smooth yield surface are well implemented in the finite element program and they can be used effectively to predict the mechanical behavior of anisotropic and asymmetric materials.

Conclusions

The modified Coulomb-Mohr yield criterion was developed by introducing anisotropic transformation to include anisotropic as well as asymmetric properties of composite materials. The modified yield surface is isotropic function of the principal values of a symmetric matrix which was transformed from the Cauchy stress. In this paper, the stress update algorithms based on the elastoplastic constitutive equations was developed. Since the developed yield criterion is composed of non-smooth multi-surface the unique direction of plastic strain-rate does not exist in the corner regions. In order to perform stress integration in the corner regions, the Koiter's flow rule for the non-smooth yield surface was used and numerically implemented. In addition to the stress update algorithm, the algorithmic tangent modulus to preserve the quadratic rate of convergence was obtained for the current non-smooth yield criterion. The developed constitutive equations and numerical algorithm was implemented into the finite element program ABAQUS/Standard using the material user subroutine UMAT.

For the validation of the developed constitutive equation and numerical formulations, the isoerror maps were used on a strain controlled problem. The results showed that the errors

in the corner regions almost vanish and this is reasonably expected results. As a second example, the extension of a strip with a circular hole is presented to compare the result with well-developed Mises yield surface. In spite of the singular regions in the current yield surface, the stress and plastic strain distributions were similar to those of Mises yield criterion.

Acknowledgement

The authors of this paper would like to thank the Korea Science and Engineering Foundation (KOSEF) for sponsoring this research through the SRC/ERC Program of MOST/ KOSEF (R11-2005-065).

References

1. W. T. Koiter, "General Theorems for Elastic-plastic Solids. Progress in Solid Mechanics 6", (I. N. Sneddon and R. Hill Eds.), pp.167-221, North-Holland Publishing Company, Amsterdam, 1960.
2. D. Peric and E. A.de S. Neto, *Computer Methods in Applied Mechanics and Engineering*, **171**, 463 (1999).
3. R. Hill, *Proc. Roy. Soc. London*, **A193**, 189 (1948).
4. F. Barlat, J. C. Brem, J. W. Yoon, K. Chung, R. E. Dick, D. J. Lege, F. Pourboghrat, S. H. Choi, and E. Chu, *International Journal of Plasticity*, **19**, 1297 (2003).
5. J. W. Yoon, D. Y. Yang, and K. Chung, *Computer Methods in Applied Mechanics and Engineering*, **174**, 23 (1999).
6. W. Prager, *Proc. Inst. Mech. Eng.*, **169**, 41 (1955).
7. H. Ziegler, *Quart. Appl. Math.*, **17**, 55 (1959).
8. J. C. Simo and T. J. R. Hughes, "Computational Inelasticity", Springer-Verlag, New York, 1998.
9. R. D. Krieg and D. B. Krieg, *Journal of Pressure Vessel Technology*, **99**, 510 (1977).